Iron-filled multiwalled carbon nanotubes surface-functionalized with paramagnetic Gd (III): A candidate dual-functioning MRI contrast agent and magnetic hyperthermia structure

Peci, T; Dennis, TJS; Baxendale, M

Iron-Filled Multiwalled Carbon Nanotubes Surface-Functionalized with Paramagnetic Gd (III): a Candidate Dual-Functioning MRI Contrast Agent and Magnetic Hyperthermia Structure

Taze Peci, T. John S. Dennis, and Mark Baxendale*

School of Physics and Astronomy, Queen Mary, University of London, Mile End Road, London E1 4NS, UK

Abstract

A simple wet chemical method involving only sonication in aqueous $GdCl_3$ solution was used for surface functionalization of iron-filled multiwalled carbon nanotubes with gadolinium. Functional groups on the sidewalls produced by the sonication provide active nucleation sites for the loading of Gd^{3+} ions. Characterization by EPR, EELS, and HRTEM confirmed the presence of Gd^{3+} ions on the sidewall surface. The room temperature ferromagnetic properties of the encapsulated iron nanowire, saturation magnetization of 40 emu/g and coercivity 600 Oe, were maintained after surface functionalization. Heating functionality in an alternating applied magnetic field was quantified through the measurement of specific absorption rate: 50 W/g_{Fe} at magnetic field strength 8 kA/m and frequency of 696 kHz. These results point to candidacy for dual-functioning MRI imaging and magnetic hyperthermia structures for cancer therapy.

---

*Corresponding author. E-mail address: m.baxendale@qmul.ac.uk (M. Baxendale).

1. Introduction

Carbon nanotubes (CNTs) have potential applications in many aspects of biomedicine owing to the outstanding mechanical, optical, and electronic properties [1]. Various functionalization methods for tuning the properties to a given application have been developed. Magnetic functionalization has resulted in nanohybrids with desirable chemical, magnetic, and other physical properties for magnetic hyperthermia cancer therapy, contrast agents for magnetic resonance imaging (MRI), and magnetic carrier and drug delivery systems [1-4]. In addition to filling the central capillary of CNTs with magnetic nanostructures, benefits can be gained by surface functionalization of the inert sidewalls [5]. Generally, covalent and non-covalent modifications are frequently used to functionalize the CNT surface [6]. Covalent functionalization which is associated with the transformation of sp^2- into sp^3- hybridized bonding commonly is achieved by using both chemical modifications by strong acids and ultra-sonication pre-treatments [5]. These treatments together alter the tube walls by introducing considerable defects and dangling bonds where various functional groups (such as hydroxyl, carbonyl, carboxyl, etc.) can be covalently attached providing active nucleation site for loading of nanoparticles [7]. However, care has to be taken since strong acid treatment accompanied with sonication may result in severe damage to the sidewalls which can modify the physical properties [6]. Moreover, the properties of a sensitive filling material may be destroyed by treatment at high temperature, or strong pH values, required by some methods reported in the literature. For example, the saturation magnetisation of surface functionalized iron-filled multiwalled carbon nanotubes (Fe-MWCNTs) is dramatically lowered if functionalized via acid treatment because the iron is oxidised by the acid [2]. Also, the nanohybrids used as carriers for drug delivery or tissue

*Corresponding author. E-mail address: m.baxendale@qmul.ac.uk (M. Baxendale).

engineering often contain sensitive organic moieties anchored on the carbon nanotubes which may be similarly damaged by strong pH values or by high temperature treatment [4]. In contrast, noncovalent functionalization is achieved by coating CNTs with amphiphilic surfactant molecules or polymers using various adsorption forces, such as the van der Waals force, hydrogen bonds, electrostatic forces, and π-stacking interactions [8-10]. Non-covalent functionalization has the advantage that it could be done under relatively mild reaction conditions so the integrity of the CNT and filling material can be maintained [6]. However, for biomedical applications, the use of polymers, surfactants or specific reactants could affect the biological response [4]. Alternative, non-destructive methods for multiple-functionalization and generally application are needed to prepare surface-functionalised CNTs. Mild sonication of MWCNTs in deionized water is known to the oxidise existing -CH_n groups on outer walls, initially to –OH then to -C=O and finally to –COOH depending on the degree of local energy density delivered to the surface by the sonication [11].

Fe-MWCNTs have been studied for over decade owing to the number of potential applications. The MWCNT serves to chemically passivate the internal nanowire and prevent mechanical degradation. The structures self-organise on inert substrates exposed to the vapour-phase products of ferrocene ($Fe(C_5H5)_2$) pyrolysis at high temperature. The detail of the growth mechanism is controversial but the general features are usually expressed within a vapour-liquid-solid framework. The encapsulated ferromagnetic nanowires display high coercivity due to the shape anisotropy. The most commonly observed encapsulated crystalline nanowires are Fe_3C (ferro-

*Corresponding author. E-mail address: m.baxendale@qmul.ac.uk (M. Baxendale).

magnetic), α-Fe (ferromagnetic), and γ-Fe (paramagnetic). The synthesis and general applications of carbon nanotubes filled with ferromagnetic materials is reviewed in Ref. [12], and specifically biomedical applications in Ref. [1].

Here, we report the surface functionalization of Fe-MWCNTs with gadolinium by a single-step method characterised by rapid and easy attachment of Gd^{3+} ions onto MWCNT sidewalls: candidate hybrids for dual-functioning magnetic hyperthermia cancer therapy and MRI contrast agent structures owing to integration of both the heating element (Fe) and the paramagnetic Gd(III) .

The claim of suitability for the magnetic hyperthermia application is made on the basis of measurement of the specific absorption rate (SAR), expressed as hysteretic power dissipation per unit mass of active ferromagnetic material upon exposure to a time-varying magnetic field [13]. The clinical practice of magnetic hyperthermia cancer therapy determines the limits of magnetic field strength (<15 kA/m) and frequency (50 kHz - 1.2 MHz) for a valid SAR measurement for this application [13]. A measurable SAR is an important prerequisite for embarkation on the very long pathway - a reflection the regulatory and other technological barriers - to an eventual clinically acceptable therapy [14].

The claim of suitability for the MRI contrast agent functionality is made on the basis of direct observation of a room temperature electron paramagnetic resonance (EPR) signal that is the signature of lanthanide ions with a half filled sub-shell [15, 16]. Although pristine or low Fe-content MWCNTs function as MRI contrast agents, the most common T_1 contrast agent in clinical usage is the strongly paramagnetic Gd (III) [17, 18].

*Corresponding author. E-mail address: m.baxendale@qmul.ac.uk (M. Baxendale).

The advantage of mild pH and sonication conditions has the benefits; (i) the magnetic properties of Fe-MWCNTs are maintained after surface functionalization, which will otherwise be destroyed if a conventional acid treatment process was applied, and (ii) the method does not involve the additional use of amphiphilic surfactant molecules or polymers which could affect the biological response.

2. Experimental

2.1. *Fe-MWCNT Synthesis*

The reactor for Fe-MWCNT production comprised a horizontal quartz tube inside preheater and central-zone heating elements, Fig.1 (A). Ferrocene vapour was produced by sublimation of 58 mg of ferrocene powder in the preheater stage (185 ^{0}C). The vapour was carried in a 14 ccm argon flow into the central zone (890-940 ^{0}C) at atmospheric pressure. Ferrocene vapour is known to decompose into solid-phase Fe and hydrocarbon species at this elevated temperature according to the reaction given in Fig.1(A)[12]. The Fe-MWNTs formed by self-organisational process on smooth quartz substrates placed inside the tube within the central zone of the furnace. The three-stage formation process is represented schematically in Fig.1(B). The vapour flow time was 1.5 min; the reactor was then cooled to 500 ^{0}C and the sample annealed at this temperature for 12 hours. Finally, the reactor was cooled to room temperature at the natural rate of the furnace. The Fe-MWNT structures were then mechanically removed from the quartz substrates, Fig.1(C). Individual structures comprise an internal Fe-based nanowire encapsulated by a MWCNT, Fig. 1(D).

*Corresponding author. E-mail address: m.baxendale@qmul.ac.uk (M. Baxendale).

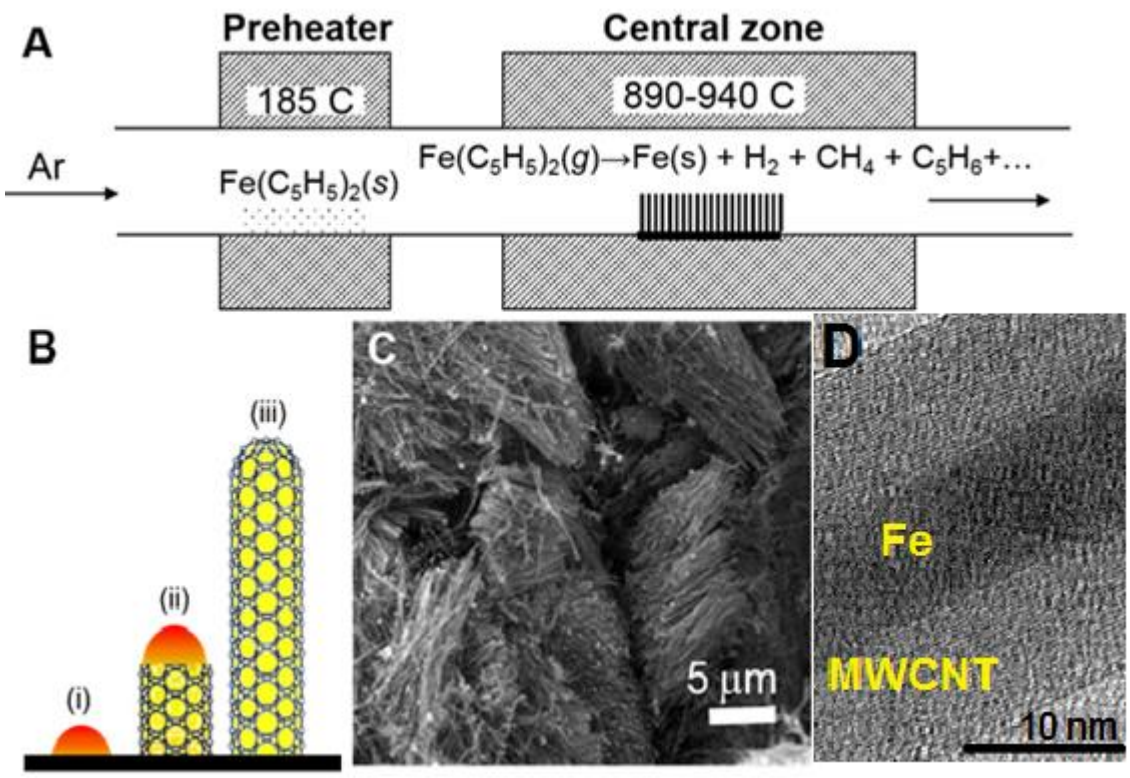

Figure 1.(A) Schematic diagram of the reactor used for Fe-MWCNT production depicting the sublimation and the products of thermal decomposition of ferrocene. The Fe-MWCNTs form and grow perpendicular to the quartz substrate located in the central zone. (B) Schematic diagram of the three-stage Fe-MWCNT nucleation and growth process (the red colouration signifies a Fe-C compound, the yellow a Fe-phase, and for clarity only a single wall of the MWCNT is depicted; (i) solid-phase Fe nucleation sites catalyse the decomposition of the ambient hydrocarbons, the carbon from the decomposition dissolves into the Fe, (ii) surface carbon initiates the MWCNT formation, and (iii) drives subsequent growth perpendicular to the substrate until the vapour feedstock ceases and the structures closes at the tip. (C) SEM image of the Fe-MWCNT powder collected after mechanical removal from the substrate. (D) TEM image of an individual Fe-MWCNT showing contrast between the encapsulated Fe nanowire and the MWCNT.

*Corresponding author. E-mail address: m.baxendale@qmul.ac.uk (M. Baxendale).

2.2. *Gd^{3+} functionalization*

50 mg of Fe-MWCNT powder and 75 mg of anhydrous gadolinium chloride ($GdCl_3$) were stirred together in 75 ml deionized water and sonicated in an 80 W ultrasonic cleaner for two hours. The solution was left undisturbed overnight whereupon the Gd^{3+} loaded Fe-MWCNTs flocculated from the solution. The supernatant solution was then decanted. The sample was washed by mild sonication in 19 ml of deionized water to remove any unabsorbed $GdCl_3$. The Gd^{3+} loaded Fe-MWCNTs flocculated again from solution and the supernatant solution was decanted. The washing procedure was repeated three times before the sample was dried in air.

2.3. *Characterization*

EPR measurements were performed at room temperature using a Bruker Elexsys E 580 spectometer, in the X frequency band (9.4GHz). EELS was performed on the Nion UltraSTEM 100, Cs corrected, dedicated scanning transmission electron microscope equipped with a Gatan Enfina EELS spectrometer. The acceleration voltage used for the experiment was 100 kV, with a probe size of 0.9 Å. The samples for EELS were prepared by transferring the structures to carbon-coated copper grids and baked at 135 ^{0}C for 6 hours. X-ray diffraction analyses were performed using a Siemens D5000 diffractometer and an Xpert-Pro diffractometer (both with Cu Kα source). For identifying and estimating the relative abundances of the phases from the area enclosed by diffraction peaks was used the Rietveld refinement method which applies the least-squares approach to match a theoretical line profile to the diffractogram. HRTEM was performed using a 200 kV Jeol Jem 2010. The samples for HRTEM were prepared by dropping a few drops of Fe-MWCNT/ethanol solution onto carbon-coated copper grids and leaving to

*Corresponding author. E-mail address: m.baxendale@qmul.ac.uk (M. Baxendale).

dry. The magnetic measurements were performed at 300 K with a Quantum Design MPMS-7 SQUID magnetometer on a powder sample. The heating functionality of Gd^{3+}-functionalized Fe-MWCNTs was studied using a Magnetherm system (NanoTherics); the sample prepared by mixing gadolinium-functionalized Fe-MWCNTs in 1:1 weight ratio with human serum albumin and dispersed in phosphate buffered saline using ultrasonication. The volume of the sample was 2 ml and the concentration was 5 mg/ml. The SAR was measured in an alternating applied magnetic field of frequency of 696 kHz and strength of 8 kA/m. The samples were handled in air for the two-month duration of the experimental work; the Gd content was directly observed in the high-vacuum conditions of the HRTEM after the two-hour 130 ^{0}C heat treatment described above. There was no time variation of the EELS chemical mapping signals, taken using a 100 keV probe, on a timescale of several hours.

3. Results and discussions

The presence of Gd^{3+} was assessed using EPR spectroscopy since the method is sensitive to paramagnetic ion content. Fig. 2 shows the EPR spectra for gadolinium functionalized Fe-MWCNTs and unfunctionalized Fe-MWNTs, both measured at room temperature.

*Corresponding author. E-mail address: m.baxendale@qmul.ac.uk (M. Baxendale).

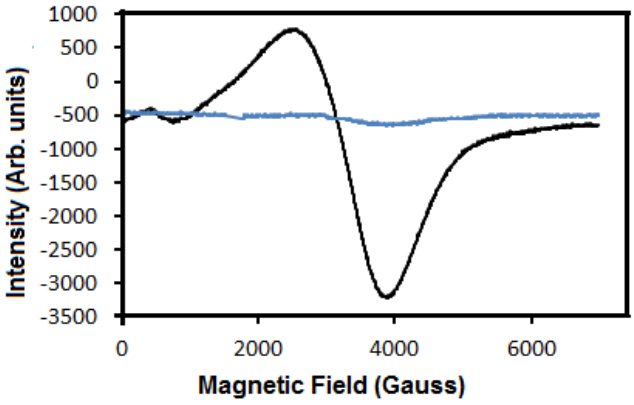

Fig. 2. EPR spectra from powder samples of gadolinium-functionalized Fe-MWCNTs and unfunctionalized Fe-MWCNTs (blue line) at 300 K.

The unfunctionalized Fe-MWCNTs signal exhibits a very weak and wide resonance in agreement with previous reports [19]. The gadolinium-functionalized Fe-MWCNTs signal is of the so-called U-spectrum type characterised by broad features [15]. Only for lanthanide ions with a half filled sub-shell, $4f^7$ (Eu^{2+}, Gd^{3+}, Tb^{4+}), L=0, S=7/2, can an EPR signal be observed at room temperature [16]. We conclude that some gadolinium present in our sample is in the Gd^{3+} state. The signal broadening is usually attributed to the dipole-dipole interaction between the Gd^{3+} ions [20]. The spectrum can be considered as the superposition of two distinct signals arising: (i) isolated ions trapped at the defect sites of MWCNTs, (ii) and clustered ions [21]. It is reported that the shape of EPR spectrum for clusters is smeared by strong dipole-dipole interaction as well as exchange coupling between closely spaced Gd^{3+} ions [20].

To investigate the spatial distribution of gadolinium in the modified Fe-MWCNTs, we performed scanning transmission electron microscopy-annular dark-field (STEM-ADF) imaging (a technique that is atomic number sensitive) in an aberration-corrected STEM with chemical

*Corresponding author. E-mail address: m.baxendale@qmul.ac.uk (M. Baxendale).

mapping by EELS. The bright-field STEM images and high-angle annular dark field (HAADF) images confirm the presence of gadolinium atoms in a surface layer of several nanometres thickness, Fig.3.

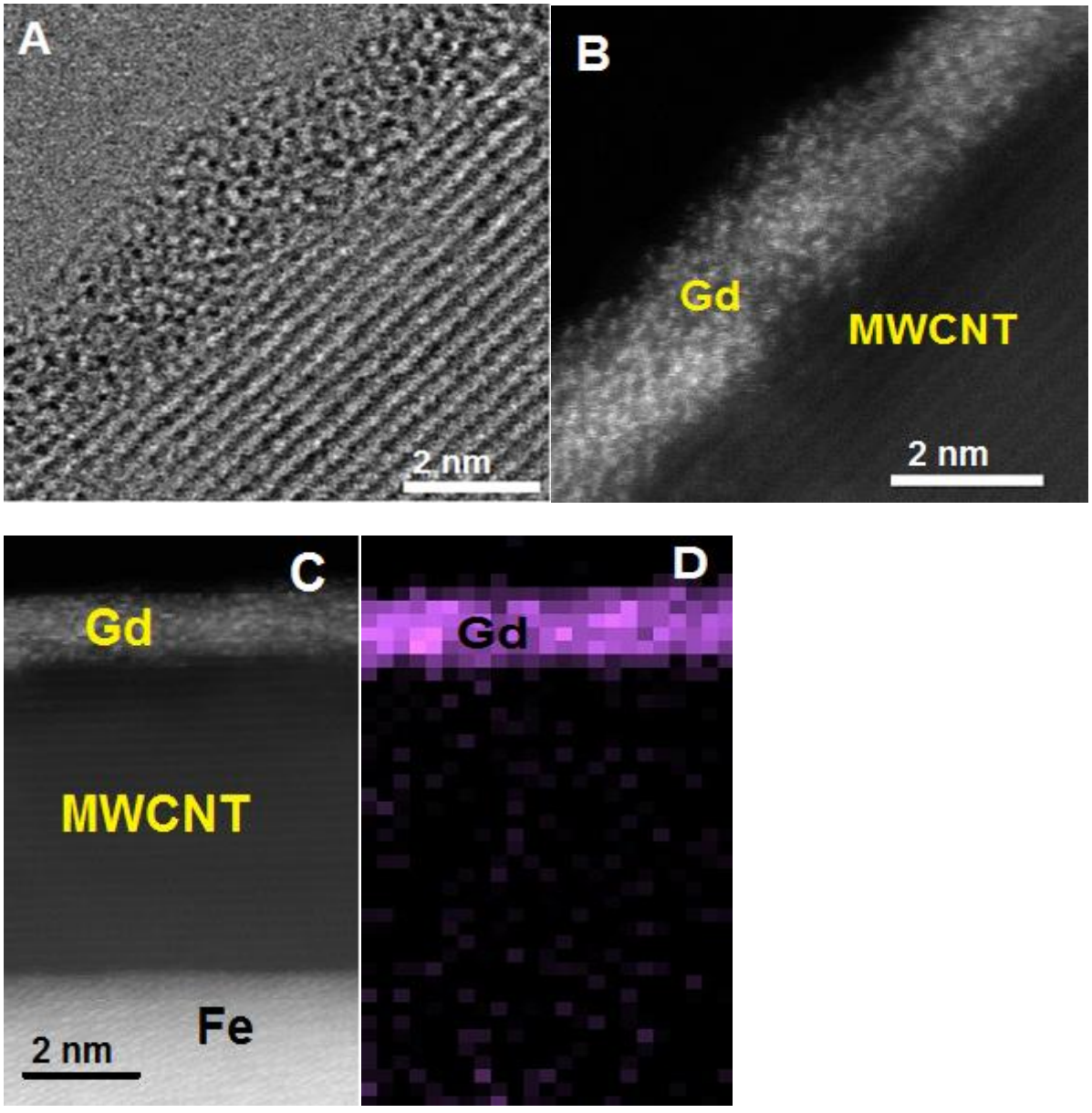

*Corresponding author. E-mail address: m.baxendale@qmul.ac.uk (M. Baxendale).

Fig. 3. (A) Typical bright-field STEM image of a gadolinium-functionalised MWCNT surface, the parallel linear features are the pristine concentric graphitic sidewalls, the surface layer of several nanometres thickness is disordered. (B) Typical HAADF image of a similar view, the image contrast is an indication of an atomic number mismatch between the pristine MWCNT regions and the surface layer. (C) Typical HAADF image of the encapsulated Fe nanowire/pristine MWCNT/surface layer. (D) The chemical map for gadolinium of the area of image (C), the bright regions indicate high density.

Fig. 4(A) shows a bright-field image of a gadolinium-functionalized Fe-MWCNT; the EELS spectra taken from locations labelled 1 and 2 and in the clearly defined pristine MWCNT walls, labelled 3, Fig. 4 (B,C).

*Corresponding author. E-mail address: m.baxendale@qmul.ac.uk (M. Baxendale).

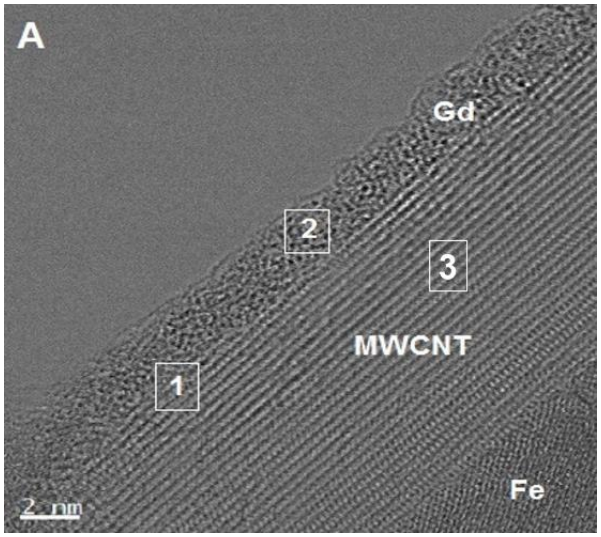

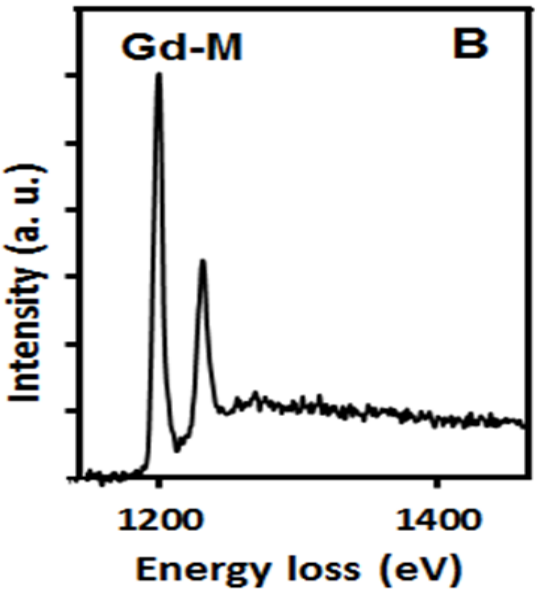

*Corresponding author. E-mail address: m.baxendale@qmul.ac.uk (M. Baxendale).

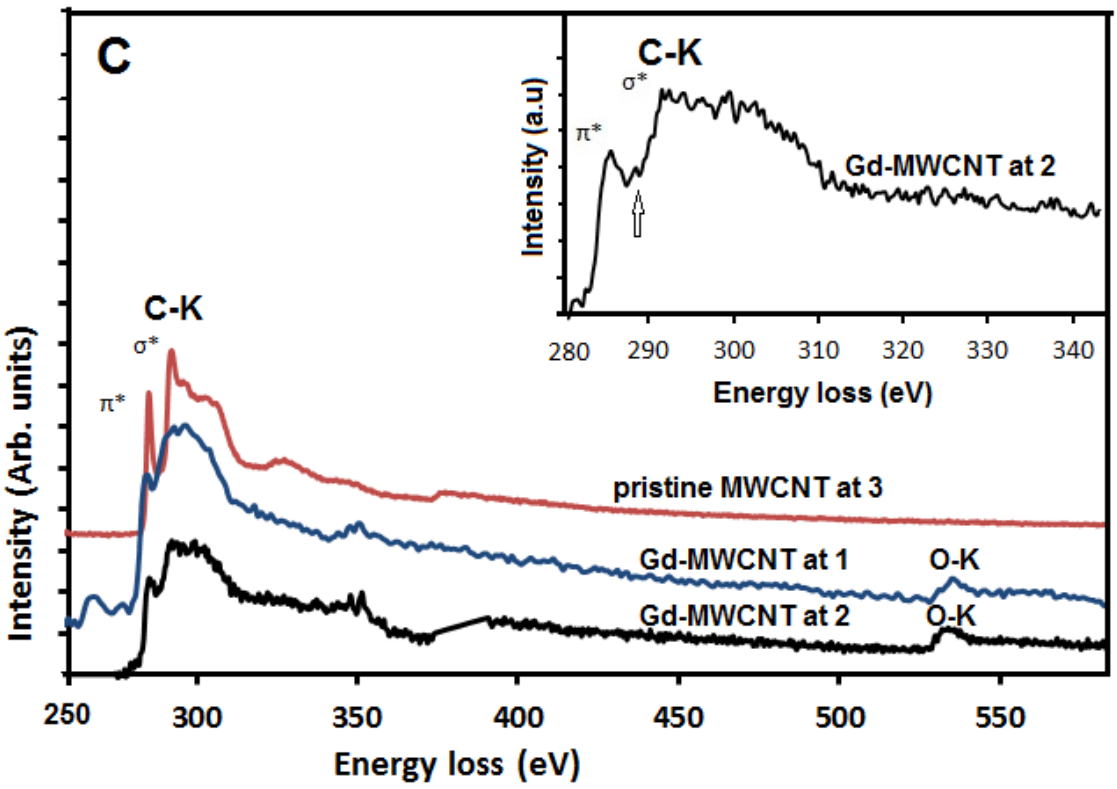

Fig. 4. (A) Bright-field image of a gadolinium-functionalized Fe-MWCNT. (B) EELS spectrum taken at location 2 in the energy range of the gadolinium M-edge features (1.185 and 1.216 eV [22]), (C) EELS spectra that shows the energy range close to the carbon K-edge and including the oxygen K-edge features recorded from the locations 1 – 3; the inset is an expansion of the location 2 spectrum, the arrow indicates the presence of a small peak at 288.4 eV. The signals were offset for ease of comparison.

The background to all spectra was subtracted by fitting a decaying power-law function to the energy window below the edge onset. The EELS spectrum obtained from the pristine MWCNT wall region closely corresponds with those reported in the literature [23]. The spectrum exhibits the spectral fingerprint of sp^2-hybridized carbon with high intensity peaks at 285 eV and 292 eV, corresponding to the excitation of a 1s core electron to the unoccupied π^* and σ^* orbitals,

*Corresponding author. E-mail address: m.baxendale@qmul.ac.uk (M. Baxendale).

respectively. In the spectrum obtained from location 1, both π* and σ* peaks from the carbon are also present but in contrast with the spectrum from pristine MWCNT region, the π* peak intensity is reduced relative to the σ* peak. A similar behaviour was observed in single-walled carbon nanotubes by X-ray absorption spectroscopy and was associated with the incorporation and release of C-O and C-H bonds [24]. This is consistent with a destruction of C-C π and σ bonds during the sonication treatment and the attachment of functional groups on the MWCNT sidewalls [5, 11]. Furthermore, the decrease of the π* peak intensity is accompanied by the smearing of the σ* peak to the higher energy features at 293 eV characteristic of the pristine MWCNT. The slight decrease of the π* peak could indicate that a small fraction of the carbon atoms form sp^3- type bonds with gadolinium atoms. This is consistent with the presence of the gadolinium in this location and with X-ray diffraction measurement which showed the presence of a small quantity (0.3%) of the gadolinium carbide phase, Fig.5. A large decrease of the π* and σ* peaks intensity accompanied by a large broadening of the σ* peak it is evident in the spectrum taken at location 2. Another interesting feature of this spectrum is the presence of a small peak at 288.4 eV, between the π* and σ* peaks which is shown with an arrow in the inset of Fig. 4(c). Similar behaviour has been observed on previous XAS studies of graphite oxide and doped graphene [25, 26]. This observation supports the presence of the oxygenated groups on the sidewalls of the sonicated MWCNTs [5,11]. This is consistent with the presence of the broad oxygen K-edge feature at 535 eV which has been attributed to convolved signals from carboxyl and hydroxyl groups [27]. In contact with the water these functional groups deproto-nate, thus leaving a negatively charged carbon surface [28]. The surface charge significantly improves the interaction between the MWCNTs and metal cations [28]. Since the functional

*Corresponding author. E-mail address: m.baxendale@qmul.ac.uk (M. Baxendale).

groups attract the M^{x+} ions and the gadolinium in the sample is in the Gd^{3+} state, we conclude that it is the ionic interaction between the deprotonated carboxyl groups and Gd^{3+} ions that attaches the gadolinium to the MWCNT surface.

The X-ray diffraction (XRD) pattern obtained from gadolinium-functionalized Fe-MWCNT powder is shown in Figure 5(A). Rietveld analyses of the XRD diffractogram was used to determine the relative abundances of the components of the sample revealed α-Fe (bcc) as the dominant encapsulated Fe phase and minor presence of γ-Fe (fcc) and iron carbide (Fe_3C). The analysis also revealed the presence of the iron oxide (Fe_3O_4), gadolinium chloride ($GdCl_3$), and a small amount of gadolinium carbide (Gd_2C_3): there is no HAADF evidence for these compounds as encapsulated phases or surface-bound groups; we conclude that these components are external to the Fe-MWCNTs. The relative weight abundances were found to be: 0.5% γ-Fe, 24% α-Fe, 0.6% Fe_3C, 65% MWCNTs, 8% Fe_3O_4, 1.5% $GdCl_3$, 0.3% Gd_2C_3.

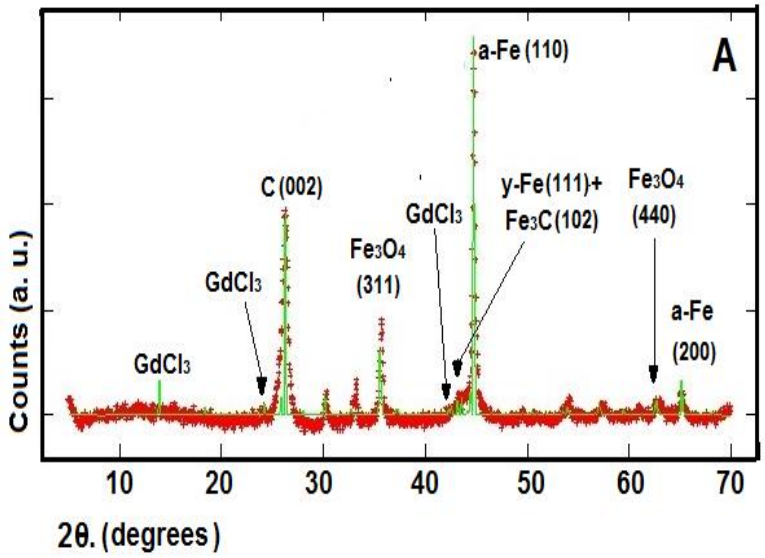

*Corresponding author. E-mail address: m.baxendale@qmul.ac.uk (M. Baxendale).

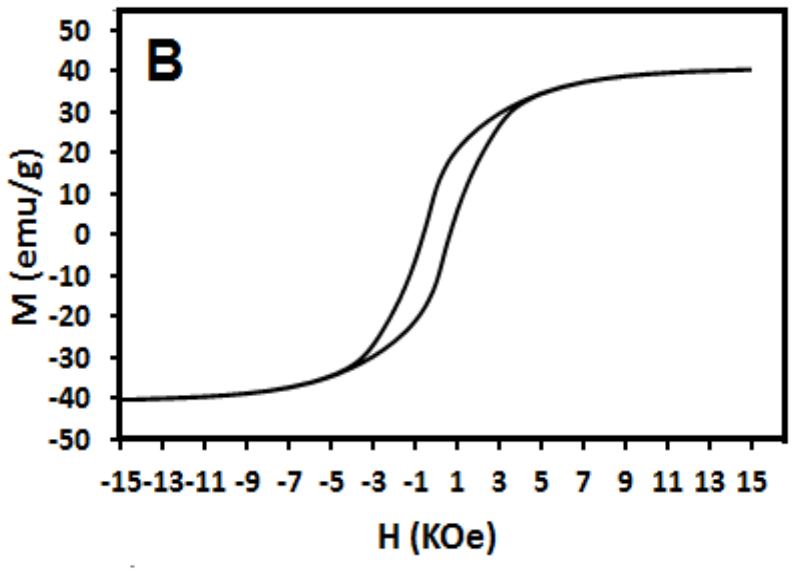

Fig. 5. (A) Typical X-ray diffractogram data (red line), and Rietveld refinement (green line) for gadolinium-functionalized Fe-MWCNTs: the refinement was made with the following components γ-Fe (Fm-3m, Crystal Open Database Ref.9008469), α-Fe (Im -3m, Crystal Open Database Ref.64998), Fe_3C (Pmna, Crystal Open Database Ref.16593), graphite (rep resenting MWCNTs) (P63/mmc, Crystal Open Database Re. 53781), Fe_3O_4 (space group Fd -3m), $GdCl_3$ (P63/m, Crystal Open Database Ref.15387), and Gd_2C_3 (I -43d, Crystal Open Database Ref. 109323). (B) The field dependence of dc magnetization at *T* = 300 K.

The magnetic field dependence of the magnetization of the gadolinium-functionalized Fe-MWCNTs powder is presented in Fig. 5(B). At room temperature, the encapsulated iron exhibited ferromagnetic hysteresis with the saturation magnetization (M_S) of 40 emu/g and a coercivity (H_C) of 600 Oe. Maintaining ferromagnetic properties of the encapsulated iron after

*Corresponding author. E-mail address: m.baxendale@qmul.ac.uk (M. Baxendale).

the surface functionalization is crucial for application of this material in magnetic hyperthermia cancer therapy.

The heating efficiency of the sample was tested in an alternating magnetic field of frequency 696 kHz and strength of 8 kA/m; the measured SAR was 50 W/g_{Fe}, where the g_{Fe} denotes the mass of the iron obtained through the relative abundance calculation described above.

4. Conclusion

We have demonstrated a simple wet chemical method involving only sonication in aqueous $GdCl_3$ solution to functionalize Fe-MWCNTs with gadolinium. This method results in loading of Gd^{3+} ions on the MWCNTs surface due to the ionic interaction between the Gd^{3+} ions and the deprotonated carboxyl groups created on the MWCNT sidewalls during the sonication process. The ferromagnetic properties of the encapsulated iron nanowire maintained after surface functionalization. A SAR of $50W/g_{Fe}$ was measured in an alternating magnetic field of frequency 696 kHz and field strength of 8 kA/m. These structures are therefore candidate hybrids for MRI imaging and magnetic hyperthermia cancer therapy with both heating functionality and integrated paramagnetic Gd (III), the most common MRI contrast agent in clinical usage.

Acknowledgments

The authors are grateful for the financial support from the Engineering and Physical Science Research Council, UK. Also, the authors are grateful to Demie Kepaptsoglou, Ray Burton-Smith, Rory M. Wilson and Russell Bailey for the help in STEM, EPR, XRD and TEM measurements respectively.

*Corresponding author. E-mail address: m.baxendale@qmul.ac.uk (M. Baxendale).

References

[1] Klingeler, R and Sim RB (Eds.) Carbon Nanotubes for Biomedical Applications, Springer 2011

[2] Hsin Y L, Lai J Y, Hwang K Ch, Lo Sh Ch, Chen F R, Kai J J. Rapid surface functionalization of iron-filled multi-walled carbon nanotubes. Carbon 2006; 44: 3328-35.

[3] Zhang H, Du N, Wu P, Chen B, Yang D. Functionalization of carbon nanotubes with magnetic nanoparticles: general nonaqueous synthesis and magnetic properties. Nanotechnology 2008; 19: 315604.

[4] Cunha C, Panseri S, Iannazzo D, Piperno A, Pistone A, Fazio M, et al. Hybrid composite made of multiwalled carbon nanotubes functionalized with Fe_3O_4 nanoparticles for tissue engineering applications. Nanotechnology 2012; 23: 465102.

[5] Rossell M D, Kuebel Ch, Ilari G, Rechberger F, Heiligtag F J, Niederberger M, *et al.* Impact of sonication pre-treatment on carbon nanotubes: A transmission electron microscopy study. Carbon 2013; 61: 404-11.

[6] Meng L, Fu Ch, Lu Q. Advanced technology for functionalization of carbon nanotubes. Progress in Natural Science 2009; 19: 801–10.

[7] Balasubramanian K, Burghard M. Chemically functionalized carbon nanotubes. Small 2005; 1: 180-92.

[8] Lefrant S, Buisson JP, Schreiber J, *et al*. Raman studies of carbon nanotubes and polymer nanotube composites. Mol. Cryst. Liq. Cryst. 2004; 415: 125–32.

*Corresponding author. E-mail address: m.baxendale@qmul.ac.uk (M. Baxendale).

[9] Nakayama-Ratchford N, Bangsaruntip S, Sun X M, *et al*. Noncovalent functionalization of carbon nanotubes by fluorescein-polyethylene glycol: supramolecular conjugates with pH-dependent absorbance and fluorescence. J. Am. Chem. Soc. 2007; 129: 2448-9.

[10] Yu J G, Huang K L, Liu S Q, et al. Preparation and characterization of polycarbonate modified multiple-walled carbon nanotubes. Chin. J. Chem. 2008; 26: 560–3.

[11] Yang D-Q, Rochette J-F, Sacher E. Functionalization of multiwalled carbon nanotubes by mild aqueous sonication. J. Phys. Chem. B 2005; 109: 7788-94.

[12] Weissker U, Hampel S, Leonhardt A, Buchner B. Carbon nanotubes filled with ferromagnetic materials. Materials 2010; 3: 4387- 427.

[13] Pankhurst QA., Connolly J, Jones SK, Dobson J. Applications of magnetic nanoparticles in biomedicine. J. Phys. D: Appl. Phys. 2003; 36: R167–R181.

[14] Pankhurst QA, Thanh NKT, Jones SK, Dobson J. Progress in applications of magnetic nanoparticles in biomedicine. J. Phys. D: Appl. Phys. 2009; 42; 224001.

[15] Simon S, Ardelean I, Filip S, Bratu I, Cosma I. Structure and magnetic properties of Bi_2O_3–GeO_3 – Gd_2O_3 glasses. Solid State Commun. 2000; 116; 83.

[16] Symons M C R. Electron Spin Resonance Part 2. Royal Society of Chemistry 1993.

[17] Ananta J S, Matson M L, Tang A M, Mandal T, Lin S, Wong K, et al. Single-walled carbon nanotubes materials as T_2 –weighted MRI contrast agents. J. Phys. Chem. C 2009; 113: 19369-72.

*Corresponding author. E-mail address: m.baxendale@qmul.ac.uk (M. Baxendale).

[18] Broome D R, Girguis M S, Baron P W, Cottrell A C, Kjellin I, Kirk G A. Gadodiamide-associated nephrogenic systemic fibrosis: why radiologists should be concerned. Am. J. Roentgenol. 2007; 188: 586-92.

[19] Sohatsky V, Kolesnik S, Makarov D, Leonhardt A, Muehl T, Moench I, *et al*. ESR of Fe-filled multi-walled carbon nanotubes. Fullerenes, Nanotubes, and Carbon Nanostructures 2005; 13: 401–10.

[20] Kliava J, Malakhovskii A, Edelman I, Potseluyko A, Petrakovskaja E, Melnikova S, *et al*. Unusual magnetic transitions and nature of magnetic resonance spectra in oxide glasses containing gadolinium. Phys. Rev. B 2005; 71: 104406.

[21] Kliava J, Edelman I S, Potseluyko A M, Petrakovskaja E A, Berger R, Bruckental I, *et al*. Magnetic and optical properties and electron paramagnetic resonance of gadolinium-containing oxide glasses. J. Phys. Condens. Matter. 2003; 15: 6671.

[22] Suenaga K, Iijima S, Kato H, Shinohara H. Fine-structure analysis of Gd M_{45} near-edge EELS on the valence state of Gd@C_{82} microcrystals. Phys. Rev. B 2000; 62: 1627-1630.

[23] Yase K, Horiuchi S, Kyotani M, Yumura M, Uchida K, Ohshima S, *et al*. Angular resolved EELS of a carbon nanotube. Thin Solid Films 1996; 273: 222-4.

[24] Abbas M, Wu Z Y, Zhong J, Ibrahim K, Fiori A, Orlanducci S, et al. X-ray absorption and photoelectron spectroscopy studies on graphite and single-walled carbon nanotubes: oxygen effect. Appl. Phys. Lett. 2005; 87: 051923.

*Corresponding author. E-mail address: m.baxendale@qmul.ac.uk (M. Baxendale).

[25] Jeong H K, Noh H J, Kim J Y, Jin M H, Park C Y, Lee Y H. X-ray absorption spectroscopy of graphite oxide. Europhysics Letters 2008**;** 82: 67004.

[26] Datsyuk V, Kalyva M, Papagelis K, Parthenios J, Tasis D, et al. Chemical oxidation of multiwalled carbon nanotubes. Carbon 2008; 46: 833-840.

[27] Zielke U, Huttinger K J, Hoffman W P. Surface-oxidized carbon fibres: I. Surface structure and chemistry. Carbon 1996; 34: 983.

[28] Tessonnier J-P, Ersen O, Weinberg G, Pham-Huu C, Su D S, Schlogl R. Selective deposition of metal nanoparticles inside or outside multiwalled carbon nanotubes. Am. Chem. Soc. 2009; 3: 2081-9.

*Corresponding author. E-mail address: m.baxendale@qmul.ac.uk (M. Baxendale).